Rapid Communication

Quasibound states in graphene quantum-dot nanostructures generated by concentric potential barrier rings*

Jiang Zhao-Tan(江兆潭)[a)†], Yu Cheng-Long(于成龙)[a)], and Dong Quan-Li(董全力)[b)]

[a)] *School of Physics, Beijing Institute of Technology, Beijing* 100081, *China*

[b)] *Beijing National Laboratory for Condensed Matter Physics, Institute of Physics, Chinese Academy of Sciences, Beijing* 100190, *China*

(Received 29 October 2011; revised manuscript received 24 November 2011)

We study the quasibound states in a graphene quantum-dot structure generated by the single-, double-, and triple-barrier electrostatic potentials. It is shown that the strongest quasibound states are mainly determined by the innermost barrier. Specifically, the positions of the quasibound states are determined by the barrier height, the number of the quasibound states is determined by the quantum-dot radius and the angular momentum, and the localization degree of the quasibound states is influenced by the width of the innermost barrier, as well as the outside barriers. Furthermore, according to the study on the double- and triple-barrier quantum dots, we find that an effective way to generate more quasibound states with even larger energy level spacings is to design a quantum dot defined by many concentric barriers with larger barrier-height differences. Last, we extend our results into the quantum dot of many barriers, which gives a complete picture about the formation of the quasibound states in the kind of graphene quantum dot created by many concentric potential barrier rings.

Keywords: electron structure of graphene, quantum dots

PACS: 73.22.Pr, 73.21.La **DOI:** 10.1088/1674-1056/21/2/027303

1. Introduction

Graphene, a typical single layer of carbon atoms with a hexagonal lattice, is attracting more and more attention due to its peculiar electronic properties.[1−7] As it is well known, the conduction and valence bands of graphene touch in a linear manner at two inequivalent Dirac points, and the charge carriers may be thought of as massless chiral fermions or massless "relativistic" electrons.[8] Thus, the so-called Klein's tunneling of a relativistic particle should be observed in graphene.[9−11] Furthermore, this indicates that the electrons can penetrate through the potential barriers of any heights without any damping.[10] Immediately, a serious challenge appears that the conventional way of fabricating electronic devices, such as quantum wells and quantum dots (QDs), by using electrostatic potentials to trap electrons will not be feasible any more.

In order to fulfill switching from the Si-base devices to the graphene-base ones, the primary step should be the reproduction of the basic unit devices. Therefore, how to fabricate QDs based on graphene is of great fundamental significance. In recent years, four different kinds of approaches of creating QDs are proposed so as to localize the electrons in the desired area: i) mechanical cutting the graphene layer into the desired shapes;[12−18] ii) switching the zero-gap band to the finite-gap one;[19−21] iii) traping electrons via magnetic confinement potential induced by the magnetic field;[22−26] iv) quasi-bounding electrons via the electrostatic potential induced by the electric field.[27−33] As a direct analog to the usual QD fabricated in a two-dimensional electron gas, the scheme of using the electrostatic potential has generated great interest due to its feasibility in adjusting and manipulating, though only quasibound states (QBS) with a finite lifetime can be obtained. Moreover, the electrostatic potential QDs can be classified according to the geometries of the QD and the shapes of the applied confinement

*Project supported by the National Natural Science Foundation of China (Grant Nos. 10974015 and 11074297) and the Program for New Century Excellent Talents in University (Grant No. NCET-08-0044).

†Corresponding author. E-mail: jiangzhaotan@hotmail.com

© 2012 Chinese Physical Society and IOP Publishing Ltd

potentials. In the continuum limit, only two typical kinds of QDs with rectangular and circular shapes are extensively investigated. The rectangular single, double, and triple QD setups have been discussed and suggested as spin qubits.[34] On the other hand, the circular single, double, and multiple QD setups defined by the smooth or sharp potentials are studied to explore their QBS. Silvestrov and Efetov studied the confinement of the quasiparticles in a QD made of a graphene strip and found that transversal electron motion plays a crucial role in electron confinement.[27] Chen *et al.*[28] investigated the Fock–Darwin states of the massless chiral fermions confined in a parabolic graphene QD with a cylindrically symmetric confinement potential and analysed the condition for the confinement of Dirac fermions. By investigating the local density of states (LDOS) of a QD confined by a cylindrically symmetric electrostatic potential with a step profile, Matulis and Peters found that some QBS are formed close to the potential barrier height.[29] In this case the larger the angular momentum, the stronger electron confining the potential exhibits. Another mechanism of electron confining is attributed to interference effects, which enable the trapping of electrons with both large and small angular momenta.[31] Furthermore, the study on the graphene QD has been extended to the double-layer QD, as well as the coupled multiple QD systems. However, to the best of our knowledge, no attention has been paid to the graphene QD formed by many concentric potential barriers with finite widths and heights.

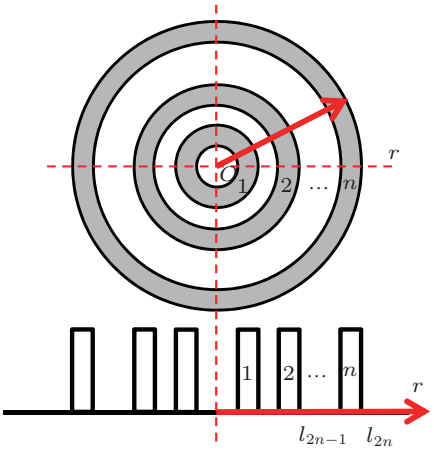


Fig. 1. (colour online) Schematic illustration of the multi-barrier graphene QD structure with circular geometrical symmetry created by the electrostatic potentials, where n denotes the number of barriers and the width of the n-th barrier is defined as the difference $d_n = l_{2n} - l_{2n-1}$.

In this work, we studied QBS in the graphene QD created by the circularly symmetric single-barrier, as well as the multi-barrier (see Fig. 1). It is shown that QBS are closely dependent on the height of potential barriers. In the case of multiple barriers with equal heights, they together form QBS. However, if the heights of the barriers are largely different, they are inclined to form QBS separately. Moreover, it is demonstrated that a single barrier only generates QBS with limited energy level spacings. QBS with relatively large energy level spacings can be created by designing the multi-barrier potential with large differences among the heights of the barriers.

The paper is organized as follows. In Section 2 we list the general procedure of determining QBS in a single-barrier QD. The corresponding discussion about the influences of the barrier parameters and the angular momentum on the bound states is carried out in detail in Section 3. Then in Section 4, we discuss QBS in double- and triple-barrier QD and finally generalize the results to the QD formed by many barriers. A conclusion is summarized in Section 5.

2. Formulation for single-barrier quantum dot

The graphene QD can be created by a single potential barrier with $n = 1$ as shown in Fig. 1. For simplicity, we adopt the dimensionless variables by introducing the unit length $l_0 = 0.1$ μm and the unit energy $E_0 = \hbar v_{\rm F}/l_0 \approx 6.58$ meV with $v_{\rm F} \approx 10^6$ m·s^{-1} the Fermi velocity. On account of the circular geometric symmetry, it is convenient to describe the QD system in the polar coordinates. Therefore, the corresponding confinement potential has the following form:

$$V(\boldsymbol{r}) = \begin{cases} 0, & r < l_1 \quad \text{(region I)}, \\ V_1, & l_1 \le r < l_2 \quad \text{(region II)}, \\ 0, & l_2 \le r < R \quad \text{(region III)}. \end{cases} \tag{1}$$

Here $V_1 > 0$ denotes the barrier height, $d_1 \equiv l_2 - l_1$ the barrier width, l_1 the QD radius, and R the radius of the whole graphene sample. Thus the Dirac-type Hamiltonian of a single electron in graphene is given by the expression[10,28–30]

$$\boldsymbol{H} = -\mathrm{i}\,\boldsymbol{\sigma}\cdot\boldsymbol{\nabla} + V(\boldsymbol{r}), \tag{2}$$

where $\boldsymbol{\sigma}$ are the Pauli matrices, and $\boldsymbol{\nabla} = (\partial_x, \partial_y)$ the in-plane gradient operator. For the Hamiltonian of the system in Eq. (2), we consider a single valley only, since the energy spectrums in two valleys near the Dirac point are degenerate. Thus we can obtain

the quasibound energy levels by solving the stationary equation

$$\boldsymbol{H}\boldsymbol{\psi}(\boldsymbol{r}) = E\boldsymbol{\psi}(\boldsymbol{r}). \tag{3}$$

Then, the Hamiltonian in Eq. (3) can be rewritten as

$$H = \begin{pmatrix} V(r) & -\mathrm{i}(\partial/\partial x - \mathrm{i}\,\partial/\partial y) \\ -\mathrm{i}(\partial/\partial x + \mathrm{i}\,\partial/\partial y) & V(r) \end{pmatrix}. \tag{4}$$

The wavefunction $\psi(\boldsymbol{r})$, corresponding to the Hamiltonian in Eq. (4), is a two-component function, where the two components correspond to the two different sublattices of the graphene honeycomb lattice. Taking into account the cylindrically symmetric confinement potential the wavefunction can be expressed in the following form[28–30]

$$\psi(r,\varphi) = \mathrm{e}^{\mathrm{i}\,m\varphi} \begin{pmatrix} a(r) \\ \mathrm{i}\,\mathrm{e}^{\mathrm{i}\,\varphi} b(r) \end{pmatrix}, \tag{5}$$

where r and φ are the polar coordinates and the integer m is the orbital angular momentum. By substituting $\psi(r,\varphi)$ into Eq. (3) we can obtain

$$\frac{\mathrm{d}b}{\mathrm{d}r} + \frac{(m+1)b}{r} + V_1 a = Ea, \tag{6a}$$

$$-\frac{\mathrm{d}a}{\mathrm{d}r} + \frac{ma}{r} + V_1 b = Eb. \tag{6b}$$

Eliminating b (or a) in the coupled differential equations in Eq. (6), we can obtain Bessel's differential equations about a (or b). Thus, the general solutions of Eq. (6) in the case of $E > 0$ are readily obtained in three regions. In region I, the solutions are expressed as $a_{\mathrm{I}} = A\,\mathrm{J}_n(Er)$ and $b_{\mathrm{I}} = A\,\mathrm{J}_{n+1}(Er)$ with J_n being the Bessel function of the n-th order; In region II, we have $a_{\mathrm{II}} = B\,\mathrm{J}_n(\varepsilon r) + C\,\mathrm{Y}_n(\varepsilon r)$ and $b_{\mathrm{II}} = \mathrm{sgn}(E - V_1)[B\,\mathrm{J}_{n+1}(\varepsilon r) + C\,\mathrm{Y}_{n+1}(\varepsilon r)]$ with Y_n being the Neumann function of the n-th order and $\varepsilon = |E - V_1|$; In region III, we further obtain $a_{\mathrm{III}} = G\,\mathrm{J}_n(Er) + H\,\mathrm{Y}_n(Er)$ and $b_{\mathrm{III}} = G\,\mathrm{J}_{n+1}(Er) + H\,\mathrm{Y}_{n+1}(Er)$. According to the continuity condition of the wavefunction at the boundaries $r = l_1$ and $r = l_2$ we derive the following relations:

$$A\,\mathrm{J}_n(El_1) = B\,\mathrm{J}_n(\varepsilon l_1) + C\,\mathrm{Y}_n(\varepsilon l_1), \tag{7a}$$

$$A\,\mathrm{J}_{n+1}(El_1) = B\,\mathrm{J}_{n+1}(\varepsilon l_1) + C\,\mathrm{Y}_{n+1}(\varepsilon l_1), \tag{7b}$$

$$B\,\mathrm{J}_n(\varepsilon l_2) + C\,\mathrm{Y}_n(\varepsilon l_2) = G\,\mathrm{J}_n(El_2) + H\,\mathrm{Y}_n(El_2), \tag{7c}$$

$$B\,\mathrm{J}_{n+1}(\varepsilon l_2) + C\,\mathrm{Y}_{n+1}(\varepsilon l_2) = G\,\mathrm{J}_{n+1}(El_2) + H\,\mathrm{Y}_{n+1}(El_2). \tag{7d}$$

To extract the information about the quasibound levels we need to impose the boundary condition $a(R) = 0$, indicating

$$G\,\mathrm{J}_n(ER) + H\,\mathrm{Y}_n(ER) = 0. \tag{8}$$

In the limit case $R \to \infty$, by using the Bessel function asymptotic expressions we have $G\cos(ER - n\pi/2 - \pi/4) + H\sin(ER - n\pi/2 - \pi/4) = 0$, which can be further written as

$$\cos\left(ER - \frac{n\pi}{2} - \frac{\pi}{4} - \theta\right) = 0 \tag{9}$$

with $\theta = \arctan(H/G)$. This demonstrates that the energy level separation is $\Delta E = \pi/R$, which is the size-confinement effect induced by R. Therefore, the energy spectrum would be continuous in the limit $R \to \infty$, which eliminates the influences caused by the sample border at R. For simplicity, the condition of Eq. (8) can be replaced by

$$G^2 + H^2 = 1. \tag{10}$$

In order to understand the peculiar properties of QBS in a QD, we closely follow the approach presented by Matulis and Peeters and obtain the LDOS as[29]

$$\rho(E) = \frac{E}{4\pi}\xi(E). \tag{11}$$

Here the integral $\xi(E)$ is defined as $\xi(E) = 2\pi\int_0^\infty r\,\mathrm{d}r F(r)|\psi(r)|^2$, where $F(r)$ is determined by the interaction between the electron and the QD. For simplicity, we substitute $F(r)$ for the aperture function $F(r) = \alpha l_1^2\,\mathrm{e}^{-\alpha r^2}$ with $\alpha = l_1^{-2}\ln 10$.[26]

Now, solving Eqs. (7) and (10) we can obtain the expressions of the coefficients A, B, C, G, and H with energy E, which are shown in Appendix A. Then inserting those coefficients into the wavefunctions in regions I, II, and III, we obtain the specific forms of the wavefunctions, which enables us to calculate the LDOS in Eq. (11).

3. Numerical results and discussions for a single-barrier quantum dot

In this section we first consider the LDOS of a single-barrier QD for the different angular momenta m, and then discuss the influences on the LDOS induced by the QD size l_1 and the barrier width d_1 (see Fig. 2). For the QD with $l_1 = 1$, $d_1 = 1$, and $V_1 = 20$, the LDOS for $m = 0, 1, \ldots, 5$ are plotted in Fig. 2(a). Obviously, some sharp peaks—the hallmark that the energy levels of QBS come into being—can

be observed in the proximity of $E = V_1$, clearly showing that QBS are formed in the QD with the energy levels near the barrier height V_1. Also, the peaks become sharper with the increase of m, indicating that the localization in the graphene QD is enhanced for the large angular momentum. This can be attributed to the fact that the orbital momenta of the electron with larger m will suppress tunneling through the barrier more strongly.[28–30] A closer look at the curves $m = 1, 3, 5$ and $m = 2, 4$ shows that the peaks become much sharper when the peak appears closer to the barrier height V_1. As proposed in Ref. [29], the incident electron and refracted electron satisfy the relation $E \sin\varphi = (V_1 - E)\sin\psi$ where φ and ψ are the angles of incidence and refraction, indicating the existence of a complete reflection critical angle φ_0, a small value in the case of $E \to V_1$. This is why the states are localized strongly in the vicinity of the top of the barrier even for orbital momentum $m = 0$.

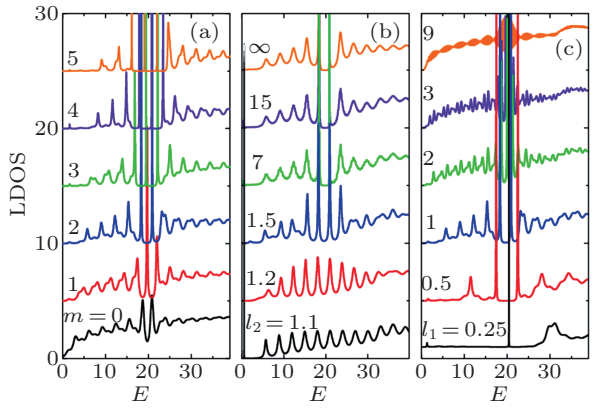


Fig. 2. (colour online) LDOS in graphene single-barrier QD with $V_1 = 20$. (a) The LDOS of the QD with $l_1 = 1$ and $l_2 = 2$ for different orbital momenta m=0, 1, ..., 5; (b) variation of the LDOS as l_2 increases from 1.1 to 15 with $l_1 = 1$ and $m = 2$, while the topmost curve corresponding to the LDOS of the QD confined by the infinite-width barrier; (c) variation of the LDOS as l_1 increases from 0.25 to 9 with $d_1 = 1$ and $m = 2$. For clarity, all the curves from bottom to top are shifted above by 0, 5, ..., 25, respectively.

Next, we examine the effect of the barrier width d_1 on QBS in Fig. 2(b). Here we select $m = 2$, $V_1 = 20$, and $l_1 = 1$. For the narrow barrier (e.g., with $d_1 = 0.1$) no sharp peaks appear, indicating that QBS with along lifetimes do not exist. Increasing the barrier width, sharp peaks come into being, verifying the appearance of long lifetime QBS. However, a further increase of d_1 after a certain barrier width (e.g. $d_1 = 7$) will not have a remarkable effect on the LDOS any more. This also verifies that the QD studied here in the limit $d_1 \to \infty$ can recover the results obtained by Matulis and Peeters,[29] as it should be, and shown by the topmost curve in Fig. 2(b). Actually, by observing the wavefunctions of the QD (not shown here), though the mechanisms of forming bound states are different, the decaying behaviors of the wavefunctions in the barrier area are the same as the wavefunction of the conventional QD confined by electrostatic potential, indicating partial information on QBS can be understood according to the picture of a conventional QD. Because the wavefunction decays quickly to almost zero in a finite barrier width and thus QBS come into being, QBS will not change any more even if d_1 is further increased.

Finally, we study QBS of the QD with different sizes l_1. For a small QD with $l_1 = 0.25$, only one quasi-bound state is formed near $E = V_1$. When the QD becomes larger in diameter, more QBS come into being. At the same time, however, the height of the LDOS peaks corresponding to QBS becoming lower, indicating that the localization of QBS become weaker. In the case of $l_1 \to \infty$, all QBS disappear. This dependence of QBS shows the qualitative similarity to the energy levels of the electron localized in the conventional potential well sandwiched between two barriers, where the energy levels will become closer to each other when the inter-barrier distance increases.

4. Results for multiple-barrier quantum dot

Aiming at the extension to the multiple-barrier QD case, we next intend to study, as examples, the double-barrier QD, as well as the triple-barrier one. Then we generalize the results to the QD with N barriers.

4.1. Double-barrier quantum dot

The double-barrier QD can be fabricated by appending another outside barrier around the barrier of the single-barrier QD. Thus the corresponding confinement potential has the following form:

$$V(\boldsymbol{r}) = \begin{cases} 0\,, & r < l_1 \quad \text{(region I)}, \\ V_1, & l_1 \le r < l_2 \quad \text{(region II)}, \\ 0\,, & l_2 \le r < l_3 \quad \text{(region III)}, \\ V_2, & l_3 \le r < l_4 \quad \text{(region IV)}, \\ 0\,, & l_4 \le r < R \quad \text{(region V)}, \end{cases} \tag{12}$$

where $V_1(V_2) > 0$ denotes the barrier height and $d_1 = l_2 - l_1 (d_2 = l_4 - l_3)$ the barrier width for the in-

ner (outer) barrier. Then the solutions of the system in different regions can be obtained readily as given in Appendix B. At the borders $r = l_1$, l_2, l_3, and l_4, the wavefunction components between adjacent regions are required to be equal and thus we obtain

$$A\,\mathrm{J}_n(El_1) = B\,\mathrm{J}_n(\varepsilon_1 l_1) + C\,\mathrm{Y}_n(\varepsilon_1 l_1), \tag{13a}$$

$$A\,\mathrm{J}_{n+1}(El_1) = B\,\mathrm{J}_{n+1}(\varepsilon_1 l_1) + C\,\mathrm{Y}_{n+1}(\varepsilon_1 l_1), \tag{13b}$$

$$B\,\mathrm{J}_n(\varepsilon_1 l_2) + C\,\mathrm{Y}_n(\varepsilon_1 l_2) = G\,\mathrm{J}_n(El_2) + H\,\mathrm{Y}_n(El_2), \tag{13c}$$

$$B\,\mathrm{J}_{n+1}(\varepsilon_1 l_2) + C\,\mathrm{Y}_{n+1}(\varepsilon_1 l_2) = G\,\mathrm{J}_{n+1}(El_2) + H\,\mathrm{Y}_{n+1}(El_2), \tag{13d}$$

$$G\,\mathrm{J}_n(El_3) + H\,\mathrm{Y}_n(El_3) = M\,\mathrm{J}_n(\varepsilon_2 l_3) + N\,\mathrm{Y}_n(\varepsilon_2 l_3), \tag{13e}$$

$$G\,\mathrm{J}_{n+1}(El_3) + H\,\mathrm{Y}_{n+1}(El_3) = M\,\mathrm{J}_{n+1}(\varepsilon_2 l_3) + N\,\mathrm{Y}_{n+1}(\varepsilon_2 l_3), \tag{13f}$$

$$M\,\mathrm{J}_n(\varepsilon_2 l_4) + N\,\mathrm{Y}_n(\varepsilon_2 l_4) = P\,\mathrm{J}_n(El_4) + Q\,\mathrm{Y}_n(El_4), \tag{13g}$$

$$M\,\mathrm{J}_{n+1}(\varepsilon_2 l_4) + N\,\mathrm{Y}_{n+1}(\varepsilon_2 l_4) = P\,\mathrm{J}_{n+1}(El_4) + Q\,\mathrm{Y}_{n+1}(El_4), \tag{13h}$$

$$P\,\mathrm{J}_n(ER) + Q\,\mathrm{Y}_n(ER) = 0. \tag{13i}$$

Note that the condition $P^2 + Q^2 = 1$ is still valid here, and $\varepsilon_1 = |E - V_1|$ and $\varepsilon_2 = |E - V_2|$.

Figure 3(a) shows the LDOS for the double-barrier QD with different barriers. We first consider QBS of a QD with two barriers having different heights ($V_1 = 20$, $V_2 = 40$) in curve B. Clearly two groups of peaks are observed near energies $E = 20$ and $E = 40$, which correspond to the heights of the two barriers V_1 and V_2, respectively. This again verifies that the formation of QBS is strongly dependent on both the barrier heights and the barrier number. Furthermore, we can find that the two sharp peaks in the vicinity of $E = V_1$ show a qualitative similarity to those of the curve in the single-barrier QD with $m = 2$ and $V = V_1$ [see Fig. 2(a)]. However, the peaks near $V_2 = 40$ have more quasibound energy levels with smaller level spacings and lower heights. This decreasing of the level spacings is attributed to the increase of the QD radius. Then we come to Fig. 3(c) and an intuitive picture about the formation of QBS from the wavefunction can be found. It is the decaying of the wavefunction components a and b (with $E \approx 39.92$) in regions IV that localizes the electron mainly in the QD with radius $r = 3$. The decaying of the wavefunction is caused mainly by the barrier with the height $V_2 = 40$ and seems to be immune to the barrier with $V_1 = 20$. As a comparison, we consider the QD constructed by the two barriers with the same heights ($V_1 = V_2 = 40$), see curve A in Fig. 3(a). Clearly the peaks at $E = 20$ disappear and the number of the peaks at $E = 40$ decreases. Note that the peaks become higher in LDOS, indicating the localizations of the electron in the QD become stronger. As shown in Fig. 3(b), the two wavefunction components a and b decrease in regions II and IV, indicating that both the two barriers together contribute to the formation of QBS. Thus we can conclude that in the case of a large enough barrier height difference the two barriers form QBS separately, while for the two barriers with the same heights both barriers together take part in the formation of QBS. Also, these results suggest a method used to generate QBS with large energy level spacings.

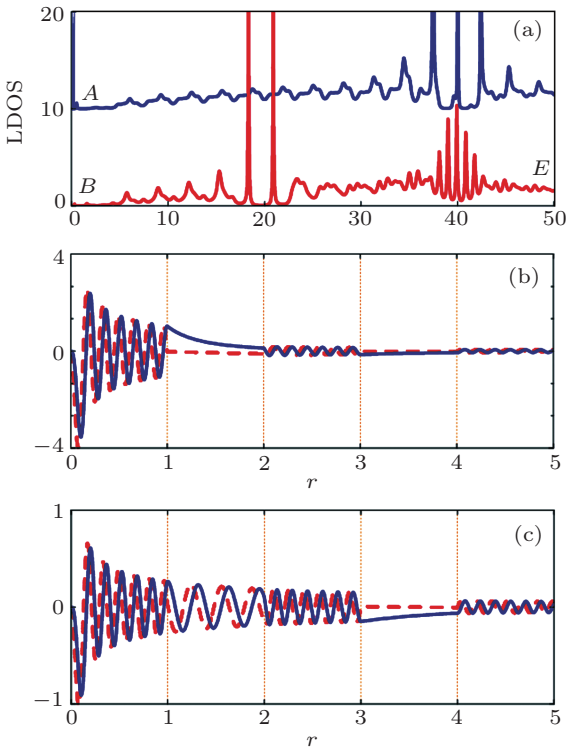


Fig. 3. (colour online) (a) LDOS in the case of $m = 2$, $l_1 = 1$, $l_2 = 2$, $l_3 = 3$, $l_4 = 4$ for the barriers $V_1 = V_2 = 40$ (curve A, blue), $V_1 = 20$ and $V_2 = 40$ (curve B, red). Components a (solid curve) and b (dashed curve) of the wavefunctions with $m = 2$ at $E \approx 39.92$ in curves A and B are shown in panels (b) and (c), respectively.

Next, to further differentiate the influences of the two barriers on QBS, we plan to elongate the distance $l_3 - l_2$ between the two barriers. In Fig. 4 we

show the variations of the LDOS versus the distance l_3-l_2 for the different barrier potential configurations. First consider the QD with the two equal barriers $V_1 = V_2 = 20$. Sharp LDOS peaks near the barrier top are observed, and seemly change little as l_3 increases from 5 to 150, even to an infinite value. This indicates that QBS are mainly caused by the inner barrier with a tiny contribution from the outer barrier in the large distance $l_2 - l_1$. Then we study the QD with two different barriers $V_1 \neq V_2$ in Figs. 4(b) and 4(c). Clearly in the small distance cases (e.g. $l_3 = 5$), two groups of peaks are observed, with one group high and sharp, and the other low and dense. The sharp peaks are almost immune to the distance $l_3 - l_2$, while the low peaks are inclined to vanish as the distance increases. Moreover, the sharp peaks are always induced by the inner barrier, while the other low peaks are induced by the outer barrier. By comparing Fig. 4(a) and Fig. 4(b), it can be found that the sharp peaks near $E = 20$ are almost kept the same, independent of the height of the outer barrier. Also, the inner barrier always forms the stronger QBS with the sharper LDOS peaks than the outer one. This further demonstrates that in the large $|V_1 - V_2|$ limit the two barriers form QBS separately, while in the $V_1 \approx V_2$ limit QBS are formed together by both barriers.

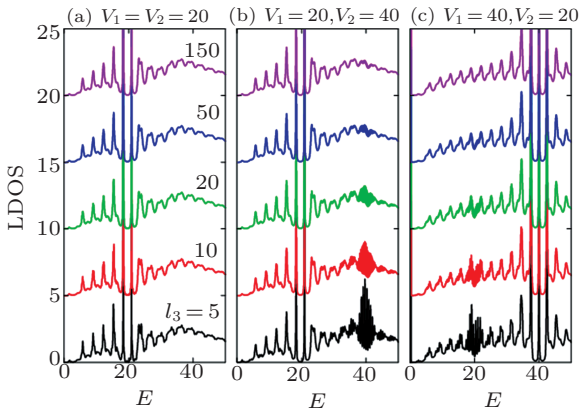


Fig. 4. (colour online) LDOS of the double-barrier QD in the case of $m = 2$, $l_1 = 1$, $l_2 = 2$, and $d_2 = 1$ for different l_3 ranging from 5 to 150 with potentials $V_1 = V_2 = 20$ (a), $V_2 = 2V_1 = 40$ (b), and $V_1 = 2V_2 = 40$ (c). For clarity, the curves from bottom to up are shifted up by 0, 5, ..., and 20, respectively.

4.2. Triple-barrier quantum dot

In order to verify the validity of the conclusion obtained by studying the double-barrier QD, we investigated QBS in the triple-barrier QD. The potential of the triple-barrier QD can be expressed as

$$V(\boldsymbol{r}) = \begin{cases} 0\,, & r < l_1 \quad \text{(region I)}, \\ V_1, & l_1 \le r < l_2 \quad \text{(region II)}, \\ 0\,, & l_2 \le r < l_3 \quad \text{(region III)}, \\ V_2, & l_3 \le r < l_4 \quad \text{(region IV)}, \\ 0\,, & l_4 \le r < l_5 \quad \text{(region V)}, \\ V_3, & l_5 \le r < l_6 \quad \text{(region VI)}, \\ 0\,, & l_6 \le r \quad \text{(region VII)}, \end{cases} \tag{14}$$

where V_1, V_2, and V_3 take positive values. The widths of the three barriers are defined as $d_1 = l_2 - l_1$, $d_2 = l_4 - l_3$, and $d_3 = l_6 - l_5$. The numerical results are shown in Fig. 5. By comparing curves A, B, and C, we can find that two sharpest peaks are obtained near $E = 20$, the top of the inner barrier, in agreement with the conclusion drawn from the

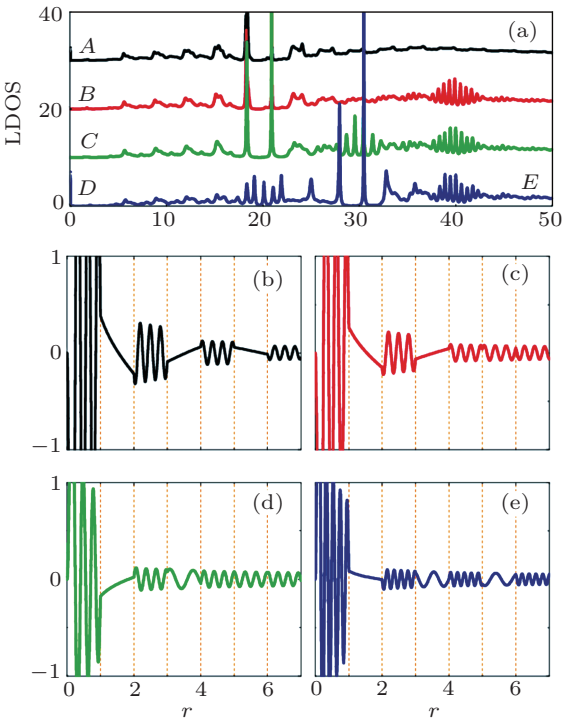


Fig. 5. (colour online) (a) LDOS of the triple-barrier QD with $m = 2$ corresponding to $V_1 = V_2 = V_3 = 20$ (curve A); $V_1 = V_2 = 20$, $V_3 = 40$ (curve B); $V_1 = 20$, $V_2 = 30$, $V_3 = 40$ (curve C); $V_1 = 30$, $V_2 = 20$, $V_3 = 40$ (curve D). For clarity curves A, B, C, and D are shifted up by 30, 20, 10, and 0, respectively. Components a of the wavefunctions corresponding the typical peaks at $E \approx 20.92$ in curve A, at $E \approx 20.92$ in curve B, at $E \approx 20.90$ in curve C, and at $E \approx 30.46$ in curve D, are plotted in panels (b), (c), (d), and (e), respectively.

double-barrier QD that the strongest QBS are mainly determined by the inner barrier. When the barrier

heights V_2 or V_3 are tuned far away from V_1, additional LDOS peaks near V_2 or V_3 will appear and, however, are lower and denser [see curve C in Fig. 5(a)]. As expected, the peaks near V_1 in the LDOS curve change little, which can also be seen clearly from the wavefunctions in Figs. 5(b)–5(d). The decaying of the wavefunction mainly appear in the region of the innermost barrier. The middle barrier, as well as the outer one, will show considerable suppressing on the wavefunction only when their heights are almost equal to V_1, otherwise they seem transparent for the wavefuctions. It should be emphasized that three groups of peaks will appear in the case of $V_1 \neq V_2 \neq V_3$ [see curve C in Fig. 5(a)]. If V_1 and V_2 are exchanged, the height of the innermost barrier becomes $V_1 = 30$ and as expected the sharpest LDOS peaks will appear near $E = V_1$, as shown by curve D in Fig. 5(a).

Taking account of the weak effect of the distances between the different barriers, we consider a special case with the interbarrier distances being zero, indicating the triple-barrier QD evolves into a complex single-barrier QD with three potential steps. Thus the potential can be expressed as

$$V(\boldsymbol{r}) = \begin{cases} 0\,, & r < l_1 \quad \text{(region I)}, \\ V_1, & l_1 \leq r < l_2 \quad \text{(region II)}, \\ V_2, & l_2 \leq r < l_3 \quad \text{(region III)}, \\ V_3, & l_3 \leq r < l_4 \quad \text{(region IV)}, \\ 0\,, & l_4 \leq r \quad \text{(region V)}, \end{cases} \tag{15}$$

where three barriers are connected together. In Fig. 6 both the LDOS and the wavefunctions are shown. In comparison with Fig. 5(a), we can find that LDOS are similar to those of the triple-barrier QD. Again it is demonstrated in a clear way that the interbarrier distances make little influence on QBS. However, the decay in the wavefunctions will change. In Fig. 6(a) $V_1 = V_2 = V_3$ means that the complex three-step barrier becomes one simple single-barrier QD. Thus, as expected, the wavefunction decays continuously in regions II, III, and IV, the same as one barrier with a width of 3. If we tune the barrier height V_3 from 20 to 40, the wavefunction mainly decays in regions II and III as shown in Fig. 6(c). If we further tune V_2 from 20 to 30, the wavefunction mainly decays in region II [Fig. 6(d)]. Also, if the barrier step is tuned into $V_1 = 30$, $V_2 = 20$, and $V_3 = 40$, the group of the sharpest peaks will appear near $E = 30$, and the decay of the wavefunctions are mainly in region II. Thus it is clearly demonstrated that the strongest QBS are formed by the innermost barrier, while the inter-barrier distances play trivial roles.

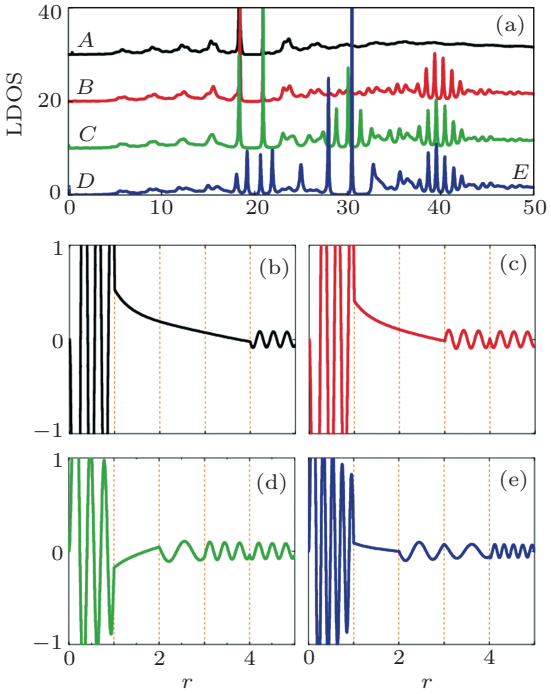


Fig. 6. (colour online) (a) LDOS of the complex single-barrier QD with $m = 2$, $l_2 = 2$, $l_3 = 3$, $l_4 = 4$ corresponding to $V_1 = V_2 = V_3 = 20$ (curve A); $V_1 = V_2 = 20$, $V_3 = 40$ (curve B); $V_1 = 20$, $V_2 = 30$, $V_3 = 40$ (curve C); $V_1 = 30$, $V_2 = 20$, $V_3 = 40$ (curve D). For clarity curves A, B, C, and D are shifted up by 30, 20, 10, and 0, respectively. Components a of the wavefunctions corresponding the typical peaks at $E \approx 20.87$ in curve A, at $E \approx 20.88$ in curve B, at $E \approx 20.91$ in curve C, and at $E \approx 30.46$ in curve D, are plotted in panels (b), (c), (d), and (e), respectively.

4.3. Generalization to N-barrier quantum dot

Based on the results about the single-, double-, and triple-barrier graphene QD, we can readily generalize the discussions to the N-barrier QD case. In the case of $V_1 \neq V_2 \neq \cdots \neq V_N$, there will appear N groups of LDOS peaks near every barrier top. In the other case with $V_1 = V_2 = \cdots = V_N$, there will be only one group of peaks appearing at the barrier top. For general cases with M barriers having the same potential heights, there will exist $N - M + 1$ groups of LDOS peaks. In all cases, the sharpest peaks in the LDOS always appear at the top of the innermost barrier. Moreover, in order to generate QBS with large energy level spacings, an effective approach is to design the barriers with largely different heights.

5. Conclusion

In conclusion, according to the continuity of wavefunctions at the borders, we considered QBS formed in electrically defined single-, double-, and triple-barrier graphene QDs. By calculating the LDOS, we can find that QBS can be formed by the concentric potential barriers, and the numbers of the groups of the LDOS peaks are determined by the numbers of barriers and the barrier heights. Also, the energy level spacings between the groups of the LDOS peaks are strongly determined by the differences among the heights of the potential barriers. Furthermore, we find that the strongest QBS is formed by the innermost circular potential barrier. The mechanism of formation of QBS in graphene QD can be seen clearly by analyzing the decay of the components of the wavefunctions in different regions. Finally, the results are extended to the QD of the multiple-barrier structure. This work provides a complete picture of QBS formed in this kind of QD formed by many concentric potential barriers, and should be a useful reference for designing or applying the graphene QD as potential nanodevices.

Appendix A: coefficients in wavefunctions of single-barrier quantum dot

The specific expressions of the coefficients A, B, C, G, and H with energy E are derived as

$$H = (1+b^2)^{-1/2}, \quad G = bH,$$
$$C = H(\mathrm{J}_n(El_2)b + \mathrm{Y}_n(El_2))/(\mathrm{J}_n(\varepsilon l_2)a + \mathrm{Y}_n(\varepsilon l_2)),$$
$$B = aC,$$

and

$$A = C[\mathrm{J}_n(\varepsilon l_1)a + \mathrm{Y}_n(\varepsilon l_1)]/\mathrm{J}_n(El_1).$$

Here for convenience we introduce some parameters

$$a = \frac{s\,\mathrm{J}_n(El_1)\,\mathrm{Y}_{n+1}(\varepsilon l_1) - \mathrm{Y}_n(\varepsilon l_1)\,\mathrm{J}_{n+1}(El_1)}{\mathrm{J}_n(\varepsilon l_1)\,\mathrm{J}_{n+1}(El_1) - s\,\mathrm{J}_n(El_1)\,\mathrm{J}_{n+1}(\varepsilon l_1)}, \quad \text{(A1)}$$

$$b = -\frac{\mathrm{Y}_{n+1}(El_2)u_n - s\,\mathrm{Y}_n(El_2)v_n}{\mathrm{J}_{n+1}(El_2)u_n - s\,\mathrm{J}_n(El_2)v_n}, \quad \text{(A2)}$$

$$u_n = \mathrm{J}_n(\varepsilon l_2)a + \mathrm{Y}_n(\varepsilon l_2), \quad \text{(A3)}$$

$$v_n = \mathrm{J}_{n+1}(\varepsilon l_2)a + \mathrm{Y}_{n+1}(\varepsilon l_2), \quad \text{(A4)}$$

$$s = \mathrm{sgn}(E - V_1). \quad \text{(A5)}$$

Appendix B: wavefunctions in double-barrier quantum dot

Here, for the sake of extending the results to the multiple-barrier QD, we list the wavefunctions in the double-barrier QD as follows. We have

$$a_{\mathrm{I}} = A\,\mathrm{J}_n(Er), \quad b_{\mathrm{I}} = A\,\mathrm{J}_{n+1}(Er)$$

in region I,

$$a_{\mathrm{II}} = B\,\mathrm{J}_n(\varepsilon_1 r) + C\,\mathrm{Y}_n(\varepsilon_1 r),$$
$$b_{\mathrm{II}} = \mathrm{sgn}(E - V_1)[B\,\mathrm{J}_{n+1}(\varepsilon_1 r) + C\,\mathrm{Y}_{n+1}(\varepsilon_1 r)]$$

in region II,

$$a_{\mathrm{III}} = D\,\mathrm{J}_n(Er) + E\,\mathrm{Y}_n(Er),$$
$$b_{\mathrm{III}} = D\,\mathrm{J}_{n+1}(Er) + E\,\mathrm{Y}_{n+1}(Er)$$

in region III,

$$a_{\mathrm{IV}} = M\,\mathrm{J}_n(\varepsilon_2 r) + N\,\mathrm{Y}_n(\varepsilon_2 r),$$
$$b_{\mathrm{IV}} = \mathrm{sgn}(E - V_2)\{M\,\mathrm{J}_{n+1}(\varepsilon_2 r) + N\,\mathrm{Y}_{n+1}(\varepsilon_2 r)\}$$

in region IV, and

$$a_{\mathrm{V}} = P\,\mathrm{J}_n(Er) + Q\,\mathrm{Y}_n(Er),$$
$$b_{\mathrm{V}} = P\,\mathrm{J}_{n+1}(Er) + Q\,\mathrm{Y}_{n+1}(Er)$$

in region V.

References

[1] Zheng Y and Ando T 2002 *Phys. Rev.* B **65** 245420

[2] Novoselov K S, Geim A K, Morozov S V, Jiang D, Zhang Y, Dubonos S V, Grigorieva I V and Firsov A A 2004 *Science* **306** 666

[3] Novoselov K S, Geim A K, Morozov S V, Jiang D, Katsnelson M I, Grigorieva I V, Dubonos S V and Firsov A A 2005 *Nature* (London) **438** 197

[4] Zheng Y, Tan Y W, Stormer H L and Kim P 2005 *Nature* (London) **438** 201

[5] Gusynin V P and Sharapov S G 2005 *Phys. Rev. Lett.* **95** 146801

[6] Wang Z Y, Hu H F, Gu L, Wang W and Jia J F 2011 *Acta Phys. Sin.* **60** 017102 (in Chinese)

[7] Tao Q, Hu X Y and Zhu P W 2011 *Acta Phys. Sin.* **60** 097301 (in Chinese)

[8] Novoselov K S, Geim1 A K, Morozov S V, Jiang D, Katsnelson M I, Grigorieva I V, Dubonos S V and Firsov A A 2005 *Nature* (London) **438** 197

[9] Calogeracos A and Dombey N 1999 *Contemp. Phys.* **40** 313

[10] Katsnelson M I, Novoselov K S and Geim A K 2006 *Nat. Phys.* **2** 620

[11] Pereira Jr J M, Vasilopoulos P and Peeters F M 2007 *Appl. Phys. Lett.* **90** 132122

[12] Ponomarenko L A, Schedin F, Katsnelson M I, Yang R, Hill1 E W, Novoselov K S and Geim A K 2008 *Science* **320** 356

[13] Güttinger J, Stampfer C, Hellmüller S, Molitor F, Ihn T and Ensslin K 2008 *Appl. Phys. Lett.* **93** 212102

[14] Schnez S, Molitor F, Stampfer C, Güttinger J, Shorubalko I, Ihn T and Ensslin K 2009 *Appl. Phys. Lett.* **94** 012107

[15] Yamamoto T, Noguchi T and Watanabe K 2006 *Phys. Rev.* B **74** 121409

[16] Ezawa M 2007 *Phys. Rev.* B **76** 245415

[17] Fernandez-Rossier J and Palacios J J 2007 *Phys. Rev. Lett.* **99** 177204

[18] Zhang Z Z, Chang K and Peeters F M 2008 *Phys. Rev.* B **77** 235411

[19] Mak K F, Lui C H, Shan J and Heinz T F 2009 *Phys. Rev. Lett.* **102** 256405

[20] Giovannetti G, Khomyakov P A, Brocks G, Kelly P J and van den Brink J 2007 *Phys. Rev.* B **76** 073103

[21] Pereira J M, Peeters F M and Vasilopoulos P 2007 *Phys. Rev.* B **75** 125433

[22] Giavaras G, Maksym P A and Roy M 2009 *J. Phys.: Condens. Matter* **21** 102201

[23] de Martino A, Dell'Anna L and Egger R 2007 *Phys. Rev. Lett.* **98** 066802

[24] Dell'Anna L and de Martino A 2009 *Phys. Rev.* B **79** 045420

[25] Hausler W and Egger R 2009 *Phys. Rev.* B **80** 161402

[26] Ramezani Masir M, Matulis A and Peeters F M 2009 *Phys. Rev.* B **79** 155451

[27] Silvestrov P G and Efetov K B 2007 *Phys. Rev. Lett.* **98** 016802

[28] Chen H Y, Apalkov V and Chakraborty T 2007 *Phys. Rev. Lett.* **98** 186803

[29] Matulis A and Peeters F M 2008 *Phys. Rev.* B **77** 115423

[30] Hewageegana P and Apalkov V 2008 *Phys. Rev.* B **77** 245426

[31] Hewageegana P and Apalkov V 2009 *Phys. Rev.* B **79** 115418

[32] Gao S H, Ren Z Y, Guo P, Zheng J M, Du G H, Wan L J and Zheng L L 2011 *Acta Phys. Sin.* **60** 047105 (in Chinese)

[33] Pan H Z, Xu M, Chen L, Sun Y Y and Wang Y L 2011 *Acta Phys. Sin.* **59** 6443 (in Chinese)

[34] Trauzettel B, Bulaev D V, Loss D and Burkard G 2007 *Nat. Phys.* **3** 192